NASA/TM—2004-213042

Measurements of Infrared and Acoustic Source Distributions in Jet Plumes

Femi A. Agboola, James Bridges, and Naseem Saiyed
Glenn Research Center, Cleveland, Ohio

April 2004

The NASA STI Program Office . . . in Profile

Since its founding, NASA has been dedicated to the advancement of aeronautics and space science. The NASA Scientific and Technical Information (STI) Program Office plays a key part in helping NASA maintain this important role.

The NASA STI Program Office is operated by Langley Research Center, the Lead Center for NASA's scientific and technical information. The NASA STI Program Office provides access to the NASA STI Database, the largest collection of aeronautical and space science STI in the world. The Program Office is also NASA's institutional mechanism for disseminating the results of its research and development activities. These results are published by NASA in the NASA STI Report Series, which includes the following report types:

- TECHNICAL PUBLICATION. Reports of completed research or a major significant phase of research that present the results of NASA programs and include extensive data or theoretical analysis. Includes compilations of significant scientific and technical data and information deemed to be of continuing reference value. NASA's counterpart of peer-reviewed formal professional papers but has less stringent limitations on manuscript length and extent of graphic presentations.

- TECHNICAL MEMORANDUM. Scientific and technical findings that are preliminary or of specialized interest, e.g., quick release reports, working papers, and bibliographies that contain minimal annotation. Does not contain extensive analysis.

- CONTRACTOR REPORT. Scientific and technical findings by NASA-sponsored contractors and grantees.

- CONFERENCE PUBLICATION. Collected papers from scientific and technical conferences, symposia, seminars, or other meetings sponsored or cosponsored by NASA.

- SPECIAL PUBLICATION. Scientific, technical, or historical information from NASA programs, projects, and missions, often concerned with subjects having substantial public interest.

- TECHNICAL TRANSLATION. English-language translations of foreign scientific and technical material pertinent to NASA's mission.

Specialized services that complement the STI Program Office's diverse offerings include creating custom thesauri, building customized databases, organizing and publishing research results . . . even providing videos.

For more information about the NASA STI Program Office, see the following:

- Access the NASA STI Program Home Page at ***http://www.sti.nasa.gov***

- E-mail your question via the Internet to help@sti.nasa.gov

- Fax your question to the NASA Access Help Desk at 301–621–0134

- Telephone the NASA Access Help Desk at 301–621–0390

- Write to:
  NASA Access Help Desk
  NASA Center for AeroSpace Information
  7121 Standard Drive
  Hanover, MD 21076

NASA/TM—2004-213042

Measurements of Infrared and Acoustic Source Distributions in Jet Plumes

Femi A. Agboola, James Bridges, and Naseem Saiyed
Glenn Research Center, Cleveland, Ohio

National Aeronautics and
Space Administration

Glenn Research Center

April 2004

Available from

NASA Center for Aerospace Information
7121 Standard Drive
Hanover, MD 21076

National Technical Information Service
5285 Port Royal Road
Springfield, VA 22100

Available electronically at http://gltrs.grc.nasa.gov

Measurements of Infrared and Acoustic Source Distributions in Jet Plumes

Femi A. Agboola,* James Bridges, and Naseem Saiyed
National Aeronautics and Space Administration
Glenn Research Center
Cleveland, Ohio 44135

Abstract

The aim of this investigation was to use the linear phased array (LPA) microphones and infrared (IR) imaging to study the effects of advanced nozzle-mixing techniques on jet noise reduction. Several full-scale engine nozzles were tested at varying power cycles with the linear phased array setup parallel to the jet axis. The array consisted of 16 sparsely distributed microphones. The phased array microphone measurements were taken at a distance of 51.0 ft (15.5 m) from the jet axis, and the results were used to obtain relative overall sound pressure levels from one nozzle design to the other. The IR imaging system was used to acquire real-time dynamic thermal patterns of the exhaust jet from the nozzles tested. The IR camera measured the IR radiation from the nozzle exit to a distance of six fan diameters ($X/D_{FAN} = 6$), along the jet plume axis.

The images confirmed the expected jet plume mixing intensity, and the phased array results showed the differences in sound pressure level with respect to nozzle configurations. The results show the effects of changes in configurations to the exit nozzles on both the flows mixing patterns and radiant energy dissipation patterns. By comparing the results from these two measurements, a relationship between noise reduction and core/bypass flow mixing is demonstrated.

Introduction

In an effort to reduce noise from turbofan engines NASA John H. Glenn Research Center (GRC) conducted extensive experiment of new engine design concepts. The concepts investigated in this study are new separate flow nozzle designs. The study was funded under the NASA's Advanced Subsonic Technology program, performed in collaboration with NASA Langley Research Center (LaRC), and private aeronautics and aerospace industries.

The IR imaging system was used to acquire real-time dynamic thermal patterns of the exhaust jet from the engines tested during the phase 2 of the NASA Engine Validation for Noise Reduction Concepts (EVNRC). The thermal imager responds to the sum of the emitted, reflected and transmitted energies (radiosity) of the jet plume. The plume temperature is obtained by subtracting both the reflected and the transmitted energies from the plume radiosity. Although the IR-image instrumentation was primarily designed for opaque radiant targets, it can be used for non-opaque media such as the jet engine exhaust plume as well, provided the background radiance is equal to the foreground radiance and the transmitted energies are minimized. The measurements obtained showed that the IR-image can be used to determine not only the temperature, but the thermal patterns can also be used for flow visualization and analysis tool as well. For the EVNRC tests, the IR-imaging radiometer was not calibrated or setup to measure absolute jet plume temperature, but relative and normalized temperature. The IR image results that are presented in this paper are relative to the baseline nozzles. The results show the effects of changes in

* National Research Council—NASA Research Associate at Glenn Research Center.

configurations to the exit nozzles on both the flows mixing patterns and radiant energy dissipation patterns.

The linear phased array (LPA) results showed that reduction in noise level due to the nozzle configurations could be separated into contributions from the bypass exit jet, core exit jet and the potential core sources. The nozzles with the chevrons showed significant reduction in the noise level generated within the potential core and moderate reduction in the noise level at the core exit. No significant noise reduction, due to the chevrons, was observed from the bypass exit.

Facility

Testing was conducted at the Honeywell Aircraft Systems (AlliedSignal at the time of testing) remote engine testing facility outside Phoenix, Arizona. Figure 1 shows the baseline separate flow nozzles without showing the AlliedSignal engine test rig. The nozzles are mounted on the Honeywell engine model TFE731-60 Turbofan Engine, equipped with Boeing B-720 flight test nacelle.

Nine configurations of the separate flow nozzles were tested. Appendix A gives a listing of these configurations and their descriptions, along with documentation of engine thrust and engine speeds. These separate flow nozzles have the basic design characteristics provided by Saiyed, Mikkelsen and Bridges[1]. The baseline nozzle was designated 3BB, while the advanced nozzle consisting of 12 core nozzle chevrons and 24 fan nozzle chevrons was designated 3AXC. The objective of the chevrons on the nozzle trailing edges was to generate streamwise vortices that mix the high and low speed flows to reduce the highest velocities which account for most of the noise. The 3AXC nozzles consist of serrations on the fan and core nozzle that are parallel to the fan and core nozzle streamlines, respectively. Configuration 3AHC is a modification with the fan chevrons distributed over a full 360°, while the core chevrons are only distributed over 180° on the side of the observer. The 3AYC, 3AKC, 3AJC, 3ALC were modifications of the 3AXC configuration. The modifications involved bending the chevrons at slight angles, to enhance flow mixing by penetrating both the bypass and the core flows. The chevrons protrude into either the core or the bypass flow by up to 15° penetration angle with some chevrons at 0° and all are arranged in alternating pattern. The chevron penetrations are normalized using the 3AXC nozzles' default penetration angle. All together, seven different variations of penetration were tested. The TFE731-60 engine conditions are provided in tables 1 and 2.

With each configuration, the nozzles were tested at varying power levels. For this report, results from the first physical limit of the engine power settings are discussed. Table 1 shows the nominal setting at maximum engine power conditions used in the experiment.

Table 1.—TFE731-60 Max Engine Power Settings.

Engine Parameters	Value
Turbine Spool Speed(within1 percent) N1	21,000 rpm
Fan Speed, Nf = N1/2.0645	10,172 rpm
Maximum Thrust	5,400 lbf
High Pressure Turbine Discharge T	1,871 °F
High Pressure Discharge Pressure	287 psig

Table 2.—Coannular Nozzle Configuration C1.

Core Flow			**Fan Flow**		
Area in^2	PR	TT,R	Area in^2	PR	TT,R
129.6	1.42	1502	311.9	1.515	618

Bypass	**Cross**	**Translation (inch)**	
Ratio	Thrust	Core Plug	Bypass Shroud
4.46	4981 lbf	–1.40	–1.1

Data Acquisition

The phased array used in this study consists of 16 microphones with the smallest spacing equal to 4 inches, while the largest spacing, the array aperture, was 424 inches. When analyzed in terms of paired spacings, this array filled 77 out of 105 possible uniquely paired spacings. This 73 percent fill is very good compared to Ishiguro[2] and Pumphrey[3] whose work showed how to analytically optimize sensors spacings. For instance, the maximum filled-array length possible by Ishiguro[2] for 16 sensors is 72 units, or 69 percent filled. Table 3 lists the microphone array configuration.

The 424 inch (10.77 m) wide array was populated by half-inch microphones (B&K 1434) and microphone preamplifiers. The microphones were placed on the test pad of AlliedSignal Engine test rig as shown in figure 2. The array was parallel to and 50.0ft from the plume centerline on the ground plane. The engine was mounted 10.0ft above the floor, meaning that the array-to-source range is 51.0ft ~ 15.5m.

Table 3.—Linear Phased Array Design.

Microphone #	1	2	3	4	5	6	7	8
Space (unit)	0	1	2	4	7	11	16	22
Space (inch)	**0**	**4**	**8**	**16**	**28**	**44**	**64**	**88**
Microphone #	9	10	11	12	13	14	15	16
Space (unit)	29	37	46	56	67	79	92	106
Space (inch)	**116**	**148**	**184**	**224**	**268**	**316**	**368**	**424**

The data acquisition system consisted of the 16 microphones, preamplifiers, power supply, and signal filtering instrumentation. The conditioned microphone signals were recorded simultaneously at a 10KHz sample rate for a 4KHz bandwidth. The spatial resolution limits of the array, given by the aperture and spacing of the transducers put the practical high frequency limit at roughly1.7kHz. The postprocessing of the phased array signals was done using a beamforming and imaging code provided by Planning Systems Incorporated of Maclean, Virginia. A reference SPL used in determining final amplitude was obtained by averaging the SPL of all the array microphones.

For consistent results from the IR-imaging system, settings on the IR camera were kept constant as much as possible from one test to the other. The focus, location of camera and stand (constant camera to target subtended angle), temperature range, temperature scale, and temperature center were kept constant throughout the testing, making it easy to compare patterns from one record to the next. IR images covered roughly the first 6 diameters of the plume, starting with the end of the plug which was maintained slightly out of the field of view to avoid saturating the camera.

It was found that the engine's IR plume patterns were not symmetrical about the centerline as they were expected to be. Reflected radiation from the test pad may have introduced addition energies into the plume. The background radiance from the distant landscape features also may have had some influence

on the IR images. However, these were not significant compared to the radiance of the plume and do not explain the observed asymmetry in all the images. This asymmetry seems to be a feature of the engine and must be kept in mind in comparing different nozzle configurations.

Results

Figure 3 shows IR images of the EVNRC test configurations. The enhanced mixing is made evident by the greatly reduced plume radiosity as the chevrons mix low and high temperature gases to reduce overall plume temperature. Also noticeable is the slight asymmetry that may be due to actual nonuniformities in the plume. In figure 4 this reduction in temperature is quantified somewhat by plotting the IR image centerline radiosity vs. axial position relative to the baseline nozzle radiosity.

To simplify comparison of images to test configurations, the radiation distribution at maximum engine power for each configuration was integrated and normalized by the baseline nozzle configuration's radiation distribution. Figure 5 presents the reduction in total radiosity *J* from the baseline nozzle image for all configurations. The terms are defined by

$$J_k = \sum_{i=1}^{N} I_i^k \tag{1}$$

$$\left[Reduction in Radiosity\right]_k = \frac{\left(J_k - J_{Baseline}\right)}{J_{Baseline}}, \tag{2}$$

where I_i^k is the radiosity of the kth nozzle at the ith pixel of the IR image.

Figure 5 also gives the amount of penetration of each configuration to aid in correlating the mixing enhancement with penetration; penetration of both core and fan nozzle chevrons are shown separately. Comparisons between the configurations in Figure 5 show that mixing enhancement is more strongly associated with increased penetration of the core chevrons (cf. configurations 3AXC and 3AJC) than fan chevrons (configurations 3AJC and 3AKC). While 3AKC has the highest penetration on both core and fan nozzles, the additional penetration on the fan over 3AJC did not result in greater mixing.

The penetration is the same for tests 3AYC and $3AYC_{CLOCKED}$, but the core nozzle for test $3AYC_{CLOCKED}$ is clocked 7.5 degrees with respect to the fan nozzle so that the core nozzle chevrons line up between fan nozzle chevrons. Figure 5 shows that there is minimal change in the total radiosity between the two tests. However, figure 4 shows that the plume temperature along the jet centerline is slightly lower for the clocked configuration. This change is so small that it may be treated as a measure of repeatability in the data.

Prior test showed that the 3AXC configuration exhibits a cruise thrust loss coefficient of 0.49 point (ΔC_{Tr} = 0.49 percent) relative to the 3BB nozzle configuration, as reported by Saiyed[1]. It is desirable to reduce the loss coefficient further. However, this test was not accurate enough for calculating thrust loss coefficient as low as 1/2 of a percent.

The question naturally arises how well mixing enhancement correlates with noise reduction. Figure 6 addresses this question directly by plotting the reduction in total radiosity and the reduction in the reference OASPL (average OASPL from array). Although the correlation between IR reduction and noise reduction is not perfect, the overall trend is very strong, with only slight variances among the best configurations not showing complete correlation. These configurations having strong penetration, they may have produced high frequency noise from the strong mixing near the nozzle that improved mixing but increased overall noise.

Figure 7 shows where the chevrons make their impact in the acoustic source distribution. The results in this figure show the relative overall sound pressure level as a function of axial coordinate. The core nozzle outlet was located at $X/D_{FAN} \simeq 0.0 \pm 0.5$, the bypass outlet was located at $X/D_{FAN} \simeq -0.5 \pm 0.5$. There is a significant, isolated source at roughly $X/D_{FAN} \simeq -1.5$ that remains an unidentified high frequency (as will be seen later) source upstream of the bypass nozzle exit. From the figure we also see that most of the significant noise sources were contained within $X/D_{FAN} \leq 10$. Figure 7 shows that the baseline nozzles, 3BB, have dominant sources several diameters downstream while the chevrons greatly reduce this source. The differences between $3BB_{hard}$ and $3BB_{treat}$ show the most reduction in the vicinity of the nozzle, with an overall reduction resulting from the normalization by the average OASPL of the array.

When analyzed by frequency band, more information can be deduced from the spatial distributions of source density. Figure 8 through 15 present these distributions for frequency bands from 50 to 3000Hz. Close study of these figures shows how the majority of the benefit from the chevrons is in the low frequencies well downstream of the nozzle. Figure 11 through 15 also show how chevrons cause interesting variations in the distributions of high frequencies. The 800 and 1600Hz bands seem particularly susceptible to a shift in location close upstream with chevrons, moving from $x/D_{FAN} = 3$ to under 2. The important 2000Hz band has peaks both at the core nozzle exit and about $x/D_{FAN} = 1.5$, the second being well correlated with the degree of penetration of the chevrons.

Summary

In testing the effect of chevrons on a separate flow nozzle mounted to an engine, infrared thermal imaging and acoustic phased arrays were employed to document the effect of the chevrons on temperature and acoustic source distributions of the plume. Several chevron configurations were tested, varying in the degree of penetration of the chevrons into the flows. The thermal mixing and low-frequency noise reduction were well correlated, both increasing with increased chevron penetration. Thermally, the increased mixing resulted in plumes being shortened by as much as 70 percent, with up to a 50 percent reduction in total IR intensity.

The acoustic source distribution measurements confirm that the primary region of noise reduction is well downstream of the nozzle, roughly 4 to 8 fan diameters where the low frequencies peak. As was noted in scale model tests, the low frequency noise reductions were accompanied by some high frequency increases. These were measured to occur primarily within the first two fan nozzle diameter of the core nozzle exit with some increase from the fan exit plane.

References

[1] Saiyed, N.H., Mikkelsen, K.L., and Bridges, J.E., "Acoustics and Thrust of Separate-Flow Exhaust Nozzles with Mixing Devices for High-Bypass-Ratio Engines," AIAA–2000–1961, 6th AIAA/CEAS Aeroacoustic Conference, Lahaina, Hawaii, June 2000.

[2] Ishiguro, M., "Minimum Redundancy Linear Arrays for Large Number of Antennas," Radio Sci. 15, pp. 1163–1170 (1980).

[3] Pumphrey, H. C., "Design of Sparse Arrays in One, Two, and Three Dimensions," J. Acoust. Soc. Am. 93 (3), pp. 1620–1626, March 1993.

Appendix A
Detailed Description of Test Hardware and Definition of Configurations

TEST CODE	DESCRIPTION (Engine speed in rpm was within 1 percent of prescribed engine test conditions for each test)	THRUST (lbf)	N1	N2
3BB	Exhaust Nozzle Configuration # 1, (C1-engine match): 360-degree straight edge core nozzle, 360-degree straight edge fan nozzle, 13/16" core shims, no core spacer, 128.73 sq. in. core area, no fan shims, 1.1" fan spacer, 294.97 sq. in. fan area	5124	20909	31444
3BB	Exhaust Nozzle Configuration # 1, (C1-engine match): 360-degree straight edge core nozzle, 360-degree straight edge fan nozzle, 13/16" core shims, no core spacer, 128.73 sq. in. core area, no fan shims, 1.1" fan spacer, 294.97 sq. in. fan area	5204	20977	31459
3AHC	Exhaust Nozzle Configuration # 17 (C1-engine match): 180-degree straight edge / 180-degree 6 chevron core nozzle, 360-degree 24 chevron fan nozzle, 7/8" core shims, no core spacer, 128.19 sq. in. core area, 1/2" fan shims, no fan spacer, 284 sq. in. fan. Core chevron inward angle = 4.5 deg., core chevron outward angle = 10.25 deg.	5085	20967	31411
3AXC	Exhaust Nozzle Configuration # 7X (C1-engine match): 360-degree 12 chevron core nozzle, 360-degree 24 chevron fan nozzle, 15/16" core shims, no core spacer, 127.66 sq. in. core area, 1/2" fan shims, no fan spacer, 284 sq. in. fan area. Core chevron inward angle = 9.0 deg., core chevron outward angle = 10.25 deg.	5085	20975	31444
3AYC	Exhaust Nozzle Configuration # 7Y (C1-engine match): 360-degree 12 chevron core nozzle, 360-degree 24 chevron fan nozzle, 15/16" core shims, no core spacer, 127.66 sq. in. core area, 1/2" fan shims, no fan spacer, 284 sq. in. fan area. Core chevron inward angle = 9.0 deg., core chevron outward angle = 15 deg.	5075	20979	31402
3AYC Clocked	Exhaust Nozzle Configuration # 7Z (3AYC Clocked*, C1-engine match): 360-degree 12 chevron core nozzle, 360-degree 24 chevron fan nozzle, 15/16" core shims, no core spacer, 127.66 sq. in. core area, 1/2" fan shims, no fan spacer, 284 sq. in. fan area. Core chevron inward angle = 9.0 deg., core chevron outward angle = 15 deg. ***Fan exhaust nozzle clocked.***	5114	20990	31348
3AJC	Exhaust Nozzle Configuration # 7J (C1-engine match): 360-degree 12 chevron core nozzle, 360-degree 24 chevron fan nozzle, 15/16" core shims, no core spacer, 127.66 sq. in. core area, 1/2" fan shims, no fan spacer, 284 sq. in. fan area. Core chevron inward angle = 13.2 deg., core chevron outward angle = 10.25 deg.	5077	20832	31447
3AKC	Exhaust Nozzle Configuration # 7K (C1-engine match): 360-degree 12 chevron core nozzle, 360-degree 24 chevron fan nozzle, 15/16" core shims, no core spacer, 127.66 sq. in. core area, 1/2" fan shims, no fan spacer, 284 sq. in. fan area. Core chevron inward angle = 13.2 deg., core chevron outward angle = 15 deg.	4992	20764	31390
3ALC	Exhaust Nozzle Configuration # 7K (C1-engine match): 360-degree 12 chevron core nozzle, 360-degree 24 chevron fan nozzle, 15/16" core shims, no core spacer, 127.66 sq. in. core area, 1/2" fan shims, no fan spacer, 284 sq. in. fan area. Core chevron inward angle = 4.5 deg., core chevron outward angle = 15 deg.	5083	20958	31384

Figure 1.—3BB nozzle on Allied
Signal engine test stand.

Figure 2.—Microphone installation on test pad.

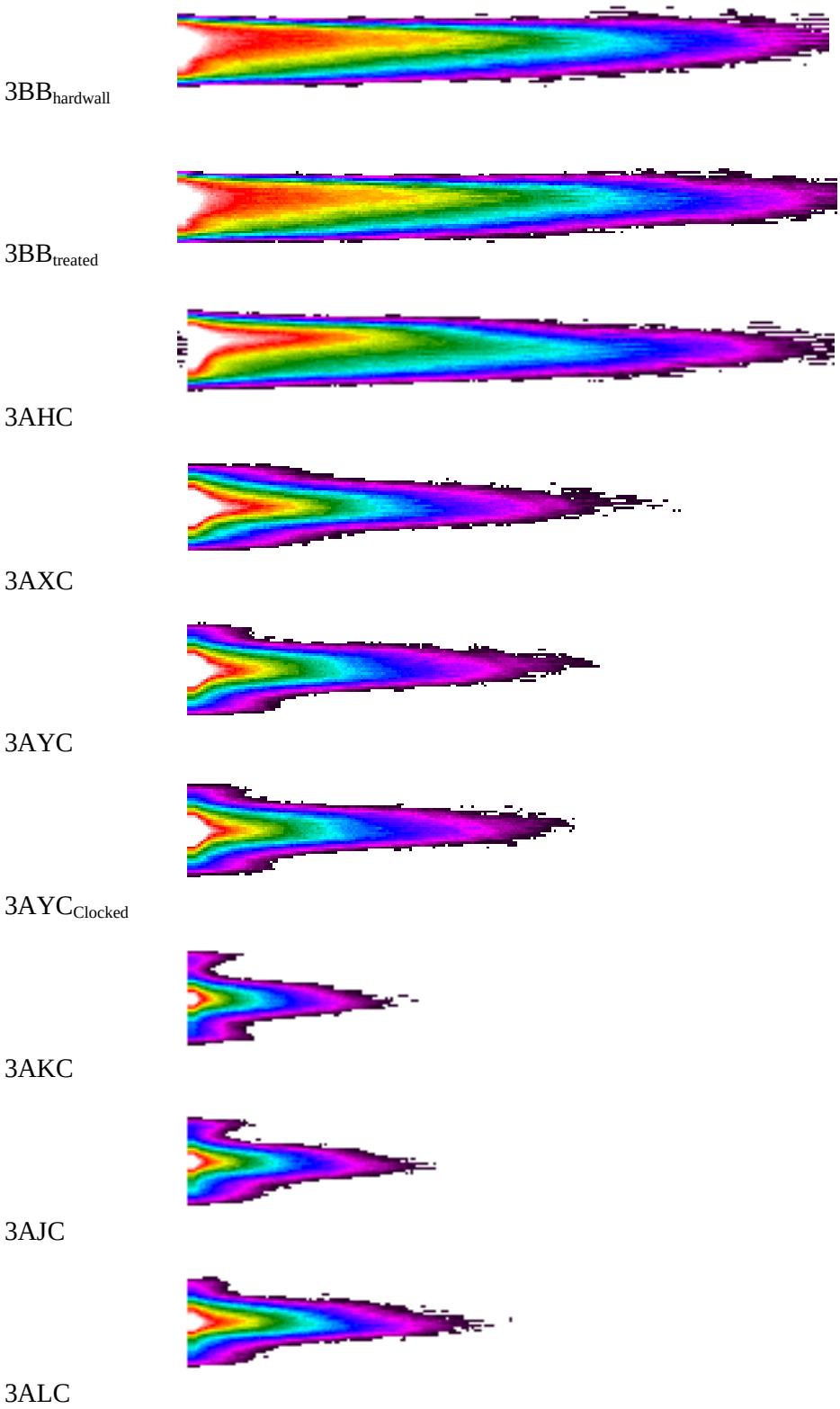

Figure 3.—IR images of the plumes from nozzles tested at maximum engine power. Engine plug located at left edge of images.

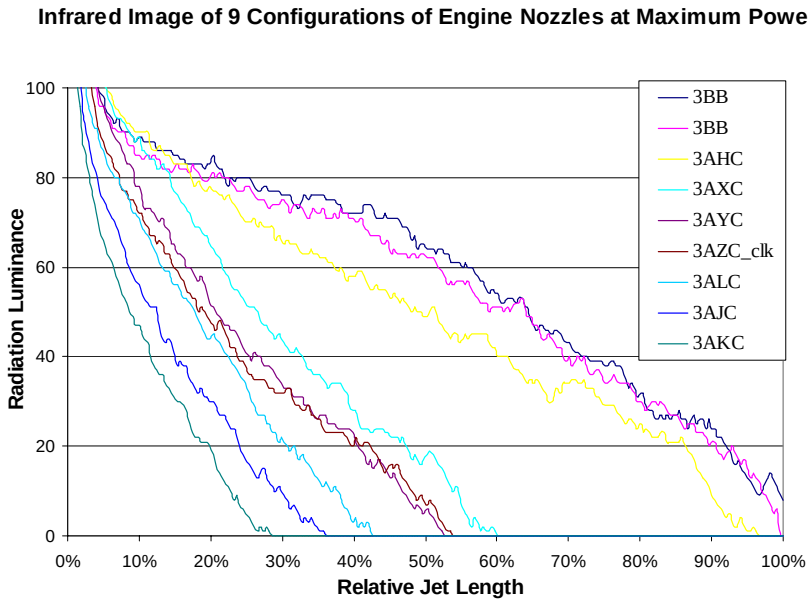

Figure 4.—IR radiosity along the jet centerline of each nozzle relative to the baseline configuration.

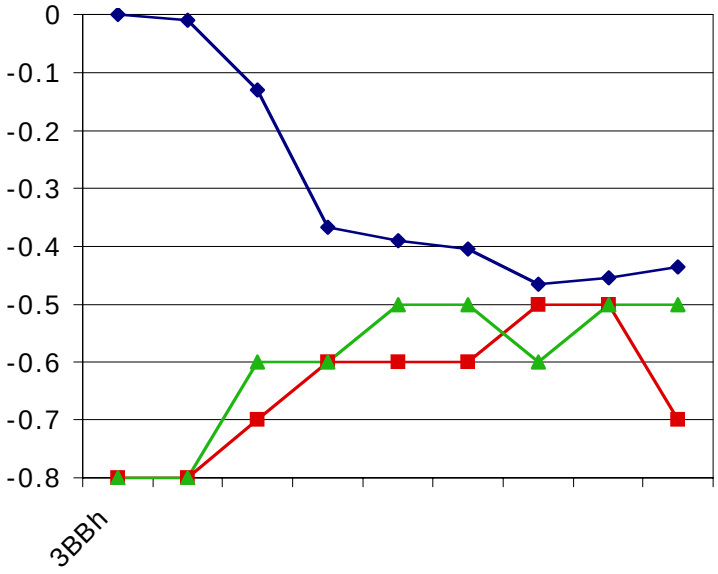

Figure 5.—Relative reduction in radiation intensity based on chevron penetration.

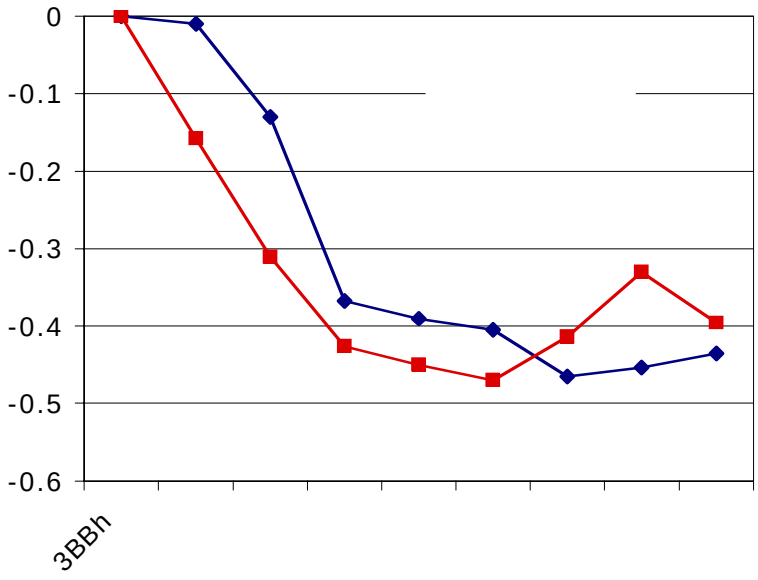

Figure 6.—Relative reduction in radiation and OASPL compared by nozzle configuration.

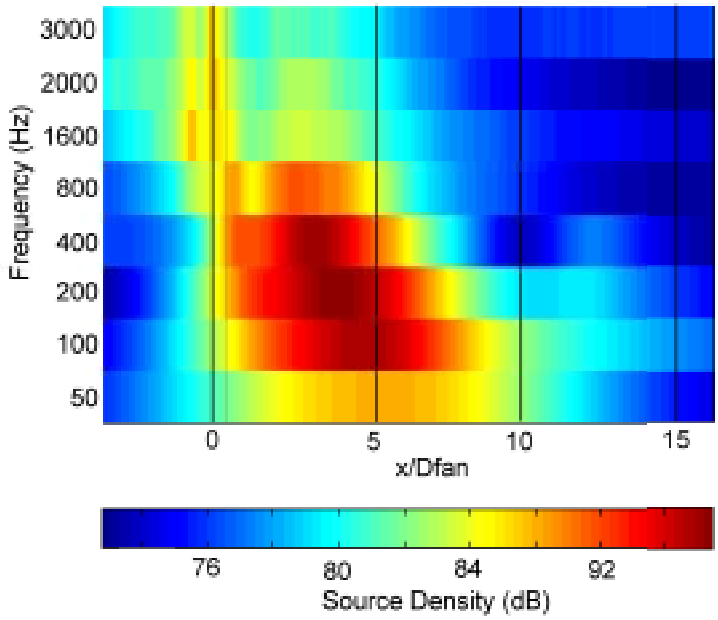

Figure 7.—Acoustic Source Density along jet axis of 3BBt.

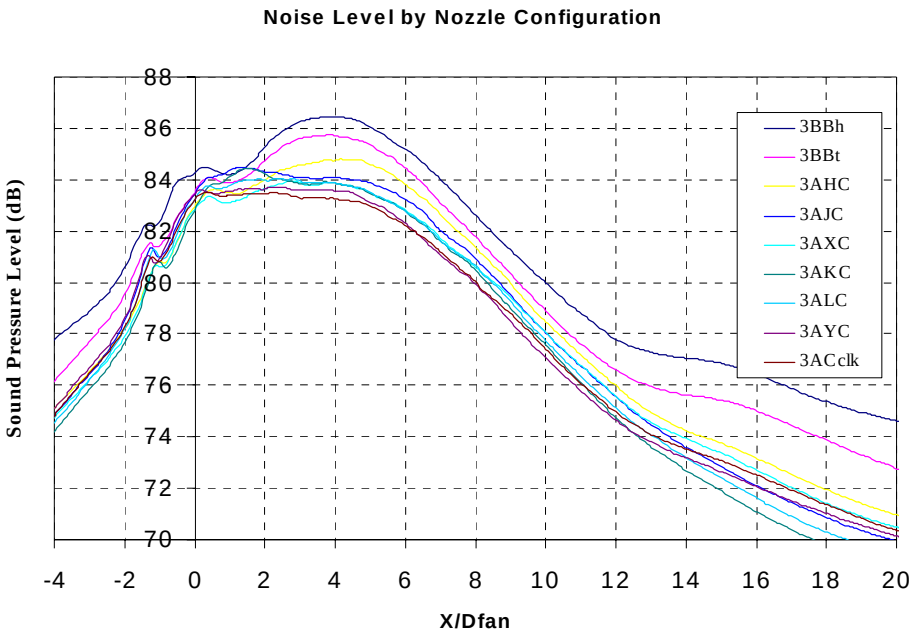

Figure 8.—Relative noise source localization along the jet axis by nozzle configuration.

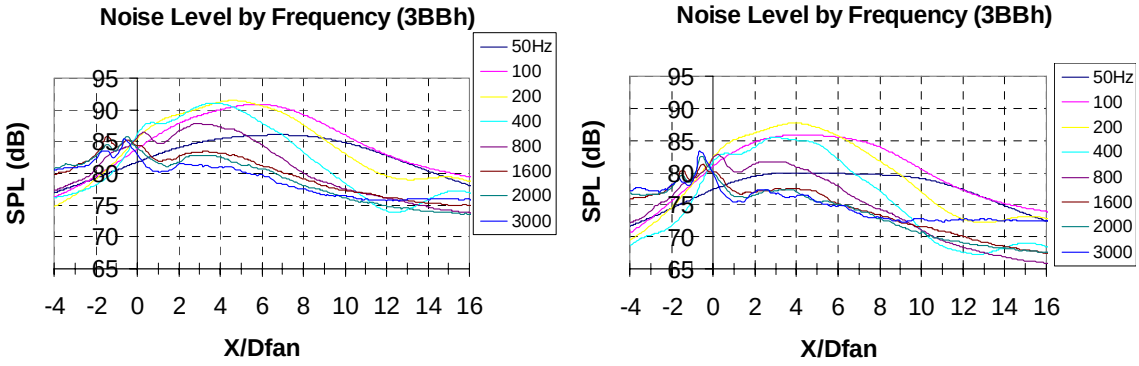

Figure 9.—Relative noise source density along the jet axis, 3BB hardwall.
100 percent (left) and 88 percent (right) engine power.

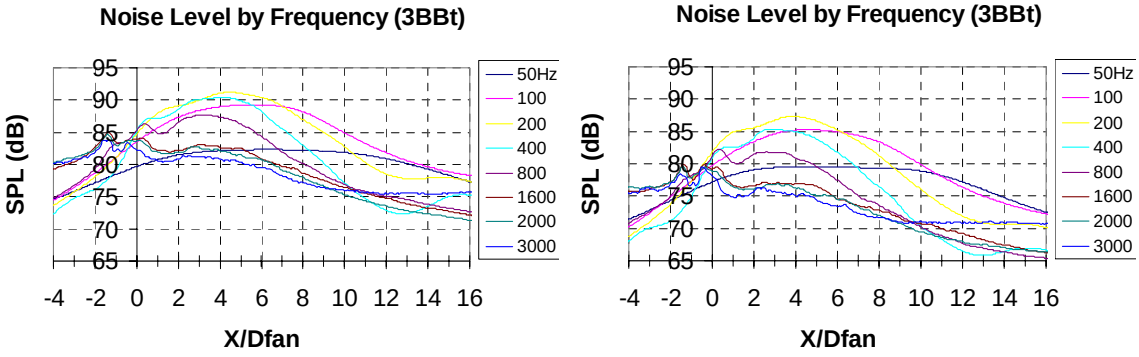

Figure 10.—Relative noise source density along the jet axis, 3BB treated wall.
100 percent (left) and 88 percent (right) engine power.

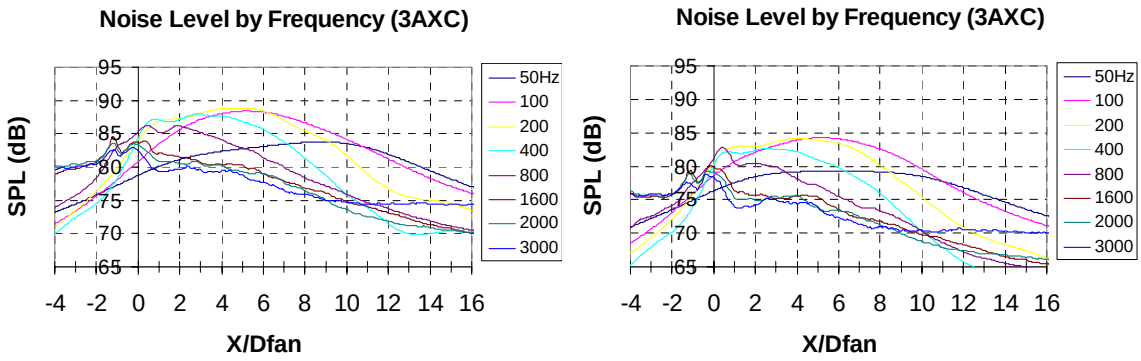

Figure 11.—Relative noise source density along the jet axis, 3AXC nozzle.
100 percent (left) and 88 percent (right) engine power.

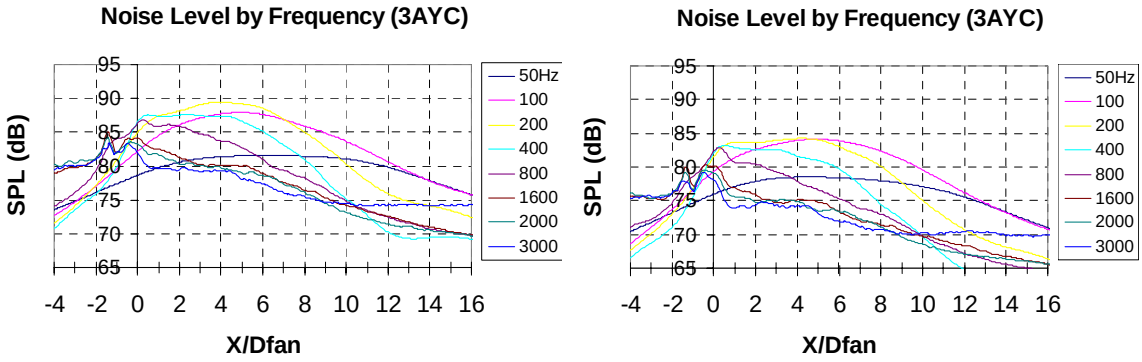

Figure 12.—Relative noise source density along the jet axis, 3AYC nozzle.
100 percent (left) and 88 percent (right) engine power..

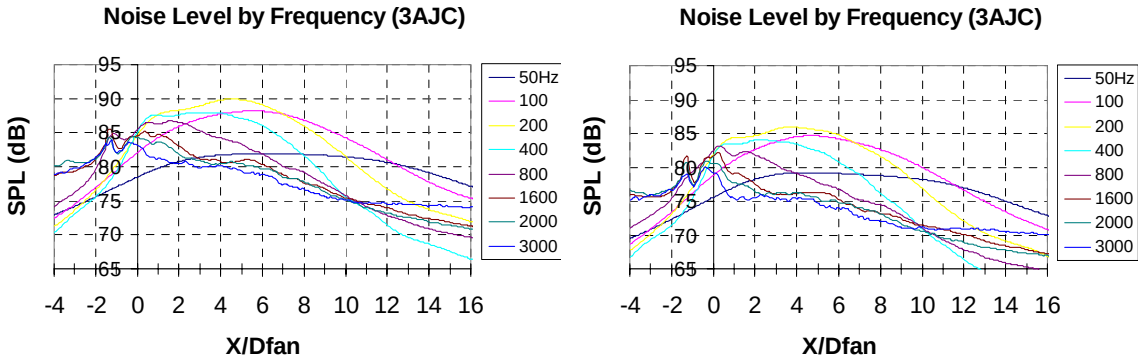

Figure 13.—Relative noise source density along the jet axis, 3AJC nozzle.
100 percent (left) and 88 percent (right) engine power.

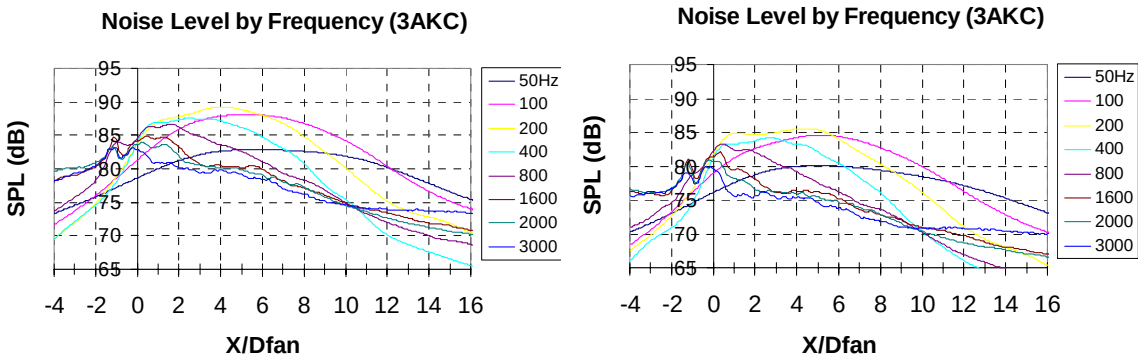

Figure 14.—Relative noise source density along the jet axis, 3AKC nozzle.
100 percent (left) and 88 percent (right) engine power.

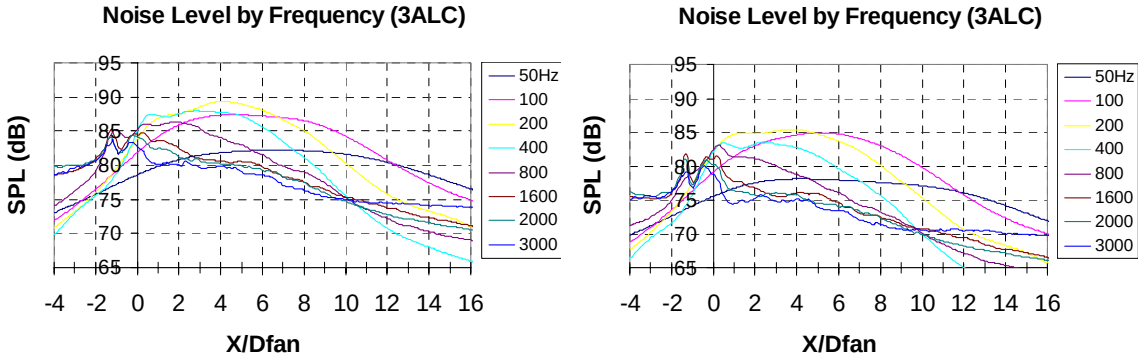

Figure 15.—Relative noise source density along the jet axis, 3ALC nozzle.
100 percent (left) and 88 percent (right) engine power.

REPORT DOCUMENTATION PAGE

Form Approved
OMB No. 0704-0188

1. AGENCY USE ONLY (*Leave blank*)	2. REPORT DATE	3. REPORT TYPE AND DATES COVERED
	April 2004	Technical Memorandum

4. TITLE AND SUBTITLE

Measurements of Infrared and Acoustic Source Distributions in Jet Plumes

5. FUNDING NUMBERS

WBS–22–781–30–27

6. AUTHOR(S)

Femi A. Agboola, James Bridges, and Naseem Saiyed

7. PERFORMING ORGANIZATION NAME(S) AND ADDRESS(ES)

National Aeronautics and Space Administration
John H. Glenn Research Center at Lewis Field
Cleveland, Ohio 44135–3191

8. PERFORMING ORGANIZATION REPORT NUMBER

E–14479

9. SPONSORING/MONITORING AGENCY NAME(S) AND ADDRESS(ES)

National Aeronautics and Space Administration
Washington, DC 20546–0001

10. SPONSORING/MONITORING AGENCY REPORT NUMBER

NASA TM—2004-213042

11. SUPPLEMENTARY NOTES

Femi A. Agboola, National Research Council—National Research Associate at Glenn Research Center; and James Bridges and Naseem Saiyed, NASA Glenn Research Center. Responsible person, James Bridges, organization code 5940, 216–433–2693.

12a. DISTRIBUTION/AVAILABILITY STATEMENT

Unclassified - Unlimited
Subject Categories: 07 and 34 Distribution: Nonstandard

Available electronically at http://gltrs.grc.nasa.gov

This publication is available from the NASA Center for AeroSpace Information, 301–621–0390.

12b. DISTRIBUTION CODE

13. ABSTRACT ***(Maximum 200 words)***

The aim of this investigation was to use the linear phased array (LPA) microphones and infrared (IR) imaging to study the effects of advanced nozzle-mixing techniques on jet noise reduction. Several full-scale engine nozzles were tested at varying power cycles with the linear phased array setup parallel to the jet axis. The array consisted of 16 sparsely distributed microphones. The phased array microphone measurements were taken at a distance of 51.0 ft (15.5 m) from the jet axis, and the results were used to obtain relative overall sound pressure levels from one nozzle design to the other. The IR imaging system was used to acquire real-time dynamic thermal patterns of the exhaust jet from the nozzles tested. The IR camera measured the IR radiation from the nozzle exit to a distance of six fan diameters ($X/D_{FAN} = 6$), along the jet plume axis. The images confirmed the expected jet plume mixing intensity, and the phased array results showed the differences in sound pressure level with respect to nozzle configurations. The results show the effects of changes in configurations to the exit nozzles on both the flows mixing patterns and radiant energy dissipation patterns. By comparing the results from these two measurements, a relationship between noise reduction and core/bypass flow mixing is demonstrated.

14. SUBJECT TERMS

Infrared imagery; Plumes; Beamforming; Suppressors; Aerodynamic noise; Coaxial nozzles; Noise reduction; Noise generators; Jet aircraft noise; Jet aircraft; Aeroacoustics; Phased arrays; Linear arrays

15. NUMBER OF PAGES

19

16. PRICE CODE

17. SECURITY CLASSIFICATION OF REPORT	18. SECURITY CLASSIFICATION OF THIS PAGE	19. SECURITY CLASSIFICATION OF ABSTRACT	20. LIMITATION OF ABSTRACT
Unclassified	Unclassified	Unclassified	